



This is a repository copy of *A low-cost metastable beta Ti alloy with high elastic admissible strain and enhanced ductility for orthopaedic application.*

White Rose Research Online URL for this paper:  
<https://eprints.whiterose.ac.uk/160379/>

Version: Published Version

---

**Article:**

Xu, Y., Gao, J., Huang, Y. et al. (1 more author) (2020) A low-cost metastable beta Ti alloy with high elastic admissible strain and enhanced ductility for orthopaedic application. *Journal of Alloys and Compounds*, 835. 155391. ISSN 0925-8388

<https://doi.org/10.1016/j.jallcom.2020.155391>

---

**Reuse**

This article is distributed under the terms of the Creative Commons Attribution (CC BY) licence. This licence allows you to distribute, remix, tweak, and build upon the work, even commercially, as long as you credit the authors for the original work. More information and the full terms of the licence here:  
<https://creativecommons.org/licenses/>

**Takedown**

If you consider content in White Rose Research Online to be in breach of UK law, please notify us by emailing [eprints@whiterose.ac.uk](mailto:eprints@whiterose.ac.uk) including the URL of the record and the reason for the withdrawal request.



[eprints@whiterose.ac.uk](mailto:eprints@whiterose.ac.uk)  
<https://eprints.whiterose.ac.uk/>



# A low-cost metastable beta Ti alloy with high elastic admissible strain and enhanced ductility for orthopaedic application



Yidong Xu, Junheng Gao<sup>\*\*</sup>, Yuhe Huang, W. Mark Rainforth<sup>\*</sup>

Department of Materials Science and Engineering, The University of Sheffield, S1 3JD, UK

## ARTICLE INFO

### Article history:

Received 11 December 2019

Received in revised form

22 April 2020

Accepted 25 April 2020

Available online 27 April 2020

### Keywords:

Metastable  $\beta$  titanium alloys

Young's modulus

Elastic admissible strain

Twinning

## ABSTRACT

In this work, a low-cost biomedical titanium alloy Ti–5Mo–Fe–3Sn (atomic percent) was successfully developed. The microstructure, tensile properties and deformation behaviour were investigated at ambient temperature. It was found that the combined addition of Sn and Fe suppressed the formation of athermal omega phase and introduced solid solution strengthening. An excellent combination of low elastic modulus (52 GPa) and high yield strength (740 MPa) was achieved, leading to a high elastic admissible strain (1.42%). Transmission electron microscopy results revealed that with an increase in tensile strain, the  $\{332\}\langle 113 \rangle$  twin system was initiated first, and then secondary  $\{332\}\langle 113 \rangle$  twinning and ternary  $\{112\}\langle 111 \rangle$  twinning were also observed. The evolution of multi-twin system during deformation was responsible for the enhanced strain hardening rate and plasticity (elongation  $\sim 30\%$ ).

© 2020 The Authors. Published by Elsevier B.V. This is an open access article under the CC BY license (<http://creativecommons.org/licenses/by/4.0/>).

## 1. Introduction

Thanks to a combination of good mechanical and biocompatible properties, Ti and its alloys are generally accepted as the best choice for implant bio-materials. However, due to the mismatch of stiffness between metallic implant and human cortical bone (10–20 GPa), governed by stress shielding, the poor bone-remodelling process can result in loosening shortly after implantation [1]. Currently, Ti–6Al–4V ELI (Ti64 ELI) and Ti–12Mo–6Zr–2Fe (TMZF) are the two most popular Ti alloys for orthopaedic applications. However, their high Young's modulus ( $\sim 110$  GPa and 80 GPa respectively), poor ductility (i.e., associated with limited working hardening) and potential toxic risk derived from metallic ion releasing (such as Al and V in Ti64) limit their further applications [2]. Therefore, the development of new Ti alloys with low Young's modulus and enhanced ductility is required. The Young's modulus of Ti alloys mainly depends on their crystal structure. Athermal  $\omega$  phase formed during quenching has the highest Young's modulus because the lattice misfit between  $\omega$  and matrix leads to higher strain at the coherent interface. Hexagonal closed packed (hcp)  $\alpha$  phase and hcp martensite ( $\alpha'$ ) exhibit a

higher Young's modulus than body-centered (bcc) phase and orthorhombic martensite ( $\alpha'$ ) [3]. Therefore, extensive work has focused on the development of metastable  $\beta$  Ti alloys through stabilizing high-temperature  $\beta$  or  $\beta+\alpha'$  to ambient temperature, such as Ti–24Nb–4Zr–8Sn (Ti2448) and Ti–29Nb–13Ta–4.6Zr (TNTZ) presenting very low Young's modulus [4–9]. However, on the basis of relatively weaker  $\beta$  stabilizing effects, most developed compositions rely on large additions of Nb and Ta, not only contributing to the accelerating price growth of raw materials, but also to increase the bulk density of implant.

Recently, enhanced plasticity in metastable beta Ti alloys has been realized via transformation induced plasticity (TRIP) and twinning induced plasticity (TWIP) effects [10,11].  $\{332\}\langle 113 \rangle$  or  $\{112\}\langle 111 \rangle$  twinning systems and stress-induced martensite (SIM) can be activated individually or simultaneously. With further deformation, the extent of twinning and/or SIM increases, which decreases the mean free path of dislocation movement, resulting in a dynamic strengthening effect. This dynamic strain hardening behaviour is well known as the dynamic “Hall-Petch” effect [10]. However, the enhanced ductility often comes at the expense of low yield strength (below 500 MPa) [11], which is ascribed to the low critical resolved shear stress (CRSS) for the formation of martensite transformation and twinning. More recently, it was found that initial deformation by primary twinning combined with the formation of martensite at a higher strain can effectively tune the strength of  $\beta$  Ti alloy via adjusting the beta phase stability [12], leading to an excellent combination of yield strength and ductility.

\* Corresponding authors.

\*\* Corresponding author.

E-mail addresses: [junheng.gao@sheffield.ac.uk](mailto:junheng.gao@sheffield.ac.uk) (J. Gao), [m.rainforth@sheffield.ac.uk](mailto:m.rainforth@sheffield.ac.uk) (W.M. Rainforth).

Considering the biocompatibility requirements of metallic implants and the synergistic effects in multicomponent alloys, it is an arduous process to obtain the balance of strength, Young's modulus and ductility. In the current work, we designed a new Ti–5Mo–Fe–3Sn (at.%) alloy with cheap alloying elements, i.e., Fe and Sn. A comparison of the mechanical behaviour between designed alloy and commercial Ti–6Al–4V ELI (Extra Low Interstitial) was carried out by the uniaxial tensile test. Here, the effects of Sn on the formation of athermal  $\omega$  phase were determined by transmission electron microscopy (TEM) and high resolution transmission electron microscopy (HRTEM). Electron backscatter diffraction (EBSD), Backscattered electron (BSE) and TEM were also performed to investigate the deformation mechanism.

## 2. Experimental

An 80 g ingot of Ti–5Mo–Fe–3Sn (at.%) was prepared via non-consumable arc melting in a high-purity argon atmosphere. After homogenization at 1373 K for 2 h under flowing argon, the ingot was hot rolled into a 4 mm-thick plate with reduction of per pass ~50% at 1273 K, followed by water quenching. Subsequently, the received plate was further cold rolled into a 2 mm-thick plate with a reduction of 50%. The as-rolled specimen was annealed at 1173 K for 10 min followed by water quenching. Meanwhile, a plate of annealed Ti–6Al–4V ELI (ASTM F136, Grade 23) was employed as a reference. These two alloys are hereafter denoted Ti513 and Ti64 ELI respectively. The BSE image of Ti64 ELI is shown in Fig. S1, exhibiting an equiaxed microstructure: transformed  $\beta$  phase is dispersed between primary  $\alpha$  grains. The composition of Ti513 was determined using an inductively coupled plasma method (ICP-OES instrument) and O content was analysed via infrared absorption (Leco ONH836 instrument), as shown in Table 1.

Flat dog-bone-shaped tensile specimens with a gauge dimension of 15 mm  $\times$  3 mm  $\times$  2 mm were prepared via Electrical Discharge Machining. Room temperature tensile tests were performed on a Zwick universal testing machine (Germany) at an initial strain rate of  $3.3 \times 10^{-4} \text{ s}^{-1}$ . A laser extensometer was used to measure the strain and corresponding Young's modulus was calculated by classic Hooke's Law during the early elastic deformation of materials. Each composition was tested at least three times to confirm the repeatability of the data.

EBSD and BSE imaging of annealed and deformed microstructure were performed on a field emission gun scanning microscopy Inspect F50 (FEI, Netherlands) and scanned at a step size of 1 and 0.2  $\mu\text{m}$  respectively. HRTEM (R005, JEOL, Japan) operating at 300 kV with a lattice resolution of 0.05 nm was employed to investigate the annealed specimen. Transmission electron microscopy (TEM) observation of deformed samples was performed on Tecnai T20 (FEI, Netherlands) operated at 200 kV. All TEM discs were prepared through twin-jet electro-polishing at  $-35 \text{ }^\circ\text{C}$  in an electrolyte consisted of 60 vol% methanol, 5 vol% perchloric acid and 35 vol% 2-butoxyethanol.

## 3. Results and discussion

The EBSD analysis of Ti513 shown in Fig. 1a shows a fully  $\beta$  equiaxed grain structure with a mean grain size of 59  $\mu\text{m}$ . The

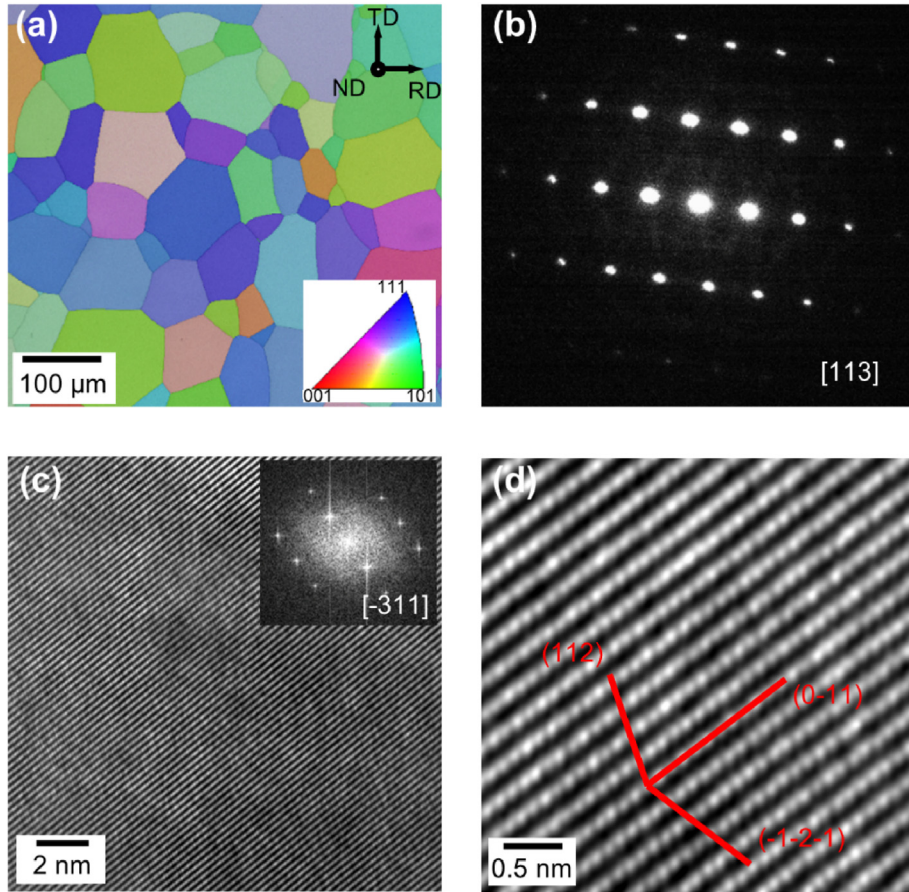
**Table 1**  
Chemical composition of fabricated Ti513 alloy in at.%.

Elements	Ti	Mo	Fe	Sn	O
Nominal composition	Bal.	5	1	3	0
Analysed composition	Bal.	4.6	1.0	3.3	0.4

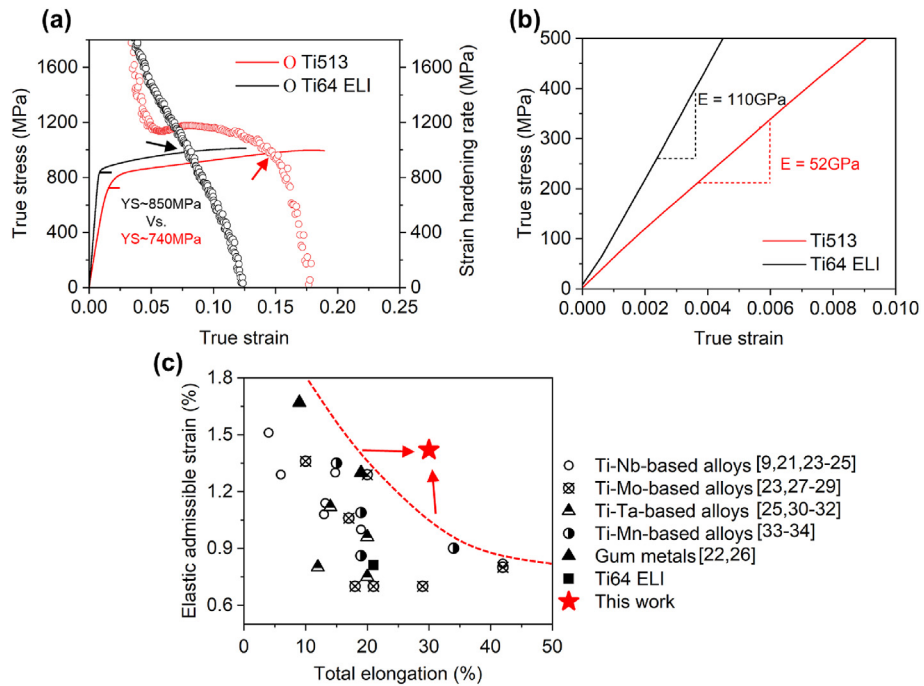
selected area electron diffraction (SAED) pattern taken along [113] zone axis (Fig. 1b) at low magnification reveals that there are no apparent  $\omega$  reflections at the 1/3 and 2/3 location between (000) and {112} reflection of  $\beta$  planes, suggesting that  $\omega$  phase is fully suppressed while quenching from high temperature. In order to present more comprehensive evidence, HRTEM image was obtained along  $[-311]$  zone axis, fast Fourier transformation (FFT) pattern (inset) as well as inverse FFT (IFFT) image in Fig. 1c–d, confirms that Ti513 has the ideal bcc structure at the atomic scale and there is no sign of the  $\omega$  phase. It has been reported that the formation of athermal  $\omega$  phase is associated with the commutative collapse of  $\{222\}_\beta$  planes in quenched metastable beta Ti alloys, and the coherent interface between  $\beta$  and athermal  $\omega$  phase fulfils the relationship of  $\langle 111 \rangle_\beta // \langle 0001 \rangle_\omega$ ,  $\{1-10\}_\beta // \{11-20\}_\omega$  [13–16]. Generally, athermal  $\omega$  phase has a dispersive distribution in the matrix and plays a significant effect on Young's modulus of the material. Therefore, as the  $\omega$  phase has been fully suppressed in this work, the low Young's modulus is retained.

Fig. 2a shows the true stress-strain curves and corresponding strain hardening rate curves of Ti513 and Ti64 ELI respectively. As indicated by the arrows, their intersection points correspond to uniform elongation. It can be seen that Ti64 ELI exhibits a high yield strength (YS,  $\sigma_{0.2}$ ) around 850 MPa and a uniform elongation close to 8%. In comparison, our Ti513 alloy presents not only a comparative YS of 740 MPa, but also a larger uniform elongation around 15%, which is almost double the value of Ti64 ELI. The strain hardening rate of the Ti64 ELI decreases monotonically and reaches zero at a strain of 12%, which is attributed to the simple deformation mechanisms involved in  $\alpha+\beta$  Ti alloys. In  $\alpha+\beta$  Ti alloys, the strain is accommodated by dislocation slip in the  $\alpha$  phase, and the consistency of glide direction in both prism and basal planes guarantees the activation of the cross-slip, resulting in low strain hardening rate [17,18]. In contrast, much stronger strain hardening behaviour is observed in Ti513. The strain hardening rate is stabilized at 1200 MPa between 5% and 12% strain. Beyond 12% strain, the strain hardening rate decreases gradually and reaches zero at 18% strain, as shown in Fig. 2a. According to the previous studies of metastable Ti alloys, the plateau of strain hardening rate was ascribed to the synergistic effects of SIM and deformation twinning [11,19,20]. To compare the difference in Young's modulus, a magnified region of the elastic deformation zone is shown in Fig. 2b, where the calculated Young's modulus of Ti513 (52 GPa) is less than half the value of Ti64 ELI (110 GPa). The elastic admissible strain, defined as the ratio of yield strength to Young's modulus, was recently considered to be an important factor of materials for orthopaedic applications. A higher value is the induction of a good balance between yield strength and Young's modulus [2,21]. The calculated elastic admissible strain of Ti513 (1.42%) is much higher than that of Ti64 ELI (0.77%), indicating a significant promise as a metallic implant. The general trend in elastic admissible strain versus ductility for recent developed biomedical Ti alloys is summarised in Fig. 2c. Clearly, Ti513 stands out from the general trend, where a high elastic admissible strain is associated with a low total elongation and visa versa [9,21–34]. More details of benchmark alloys can be found in Table S1.

To investigate the deformation mechanism of Ti513, EBSD mapping was carried out on the 10% strained sample. Fig. 3a provides the Inverse Pole Figure (IPF) and the image quality (IQ) images of the deformed microstructure. The misorientation angles between matrix and bands highlighted by the solid red lines were determined to be around  $50.5^\circ$ , corresponding to  $\{332\} \langle 113 \rangle$  twinning systems. Generally, the networking of  $\{332\}$  type twins is denser at higher strains, leading to stable strain hardening and thus the large uniform elongation. Moreover, it can be found from the BSE image in Fig. 3b that there is a high density of



**Fig. 1.** (a) EBSD Inverse pole figure, IPF + Image quality, IQ image of Ti513 after annealing. (b) Corresponding selected area diffraction pattern (SAED) along [113] zone axis. (c) HRTEM image from Ti513 and corresponding FFT pattern (inset of (c)). (d) Magnified IFFT image from (c).



**Fig. 2.** (a) True stress-true strain tensile curves and corresponding strain hardening rates of Ti513 and Ti64 ELI respectively. (b) Magnified image of elastic deformation zone of Ti513 and Ti64 ELI respectively. (c) Comparison of elastic admissible strain and elongation in various established Ti alloys.

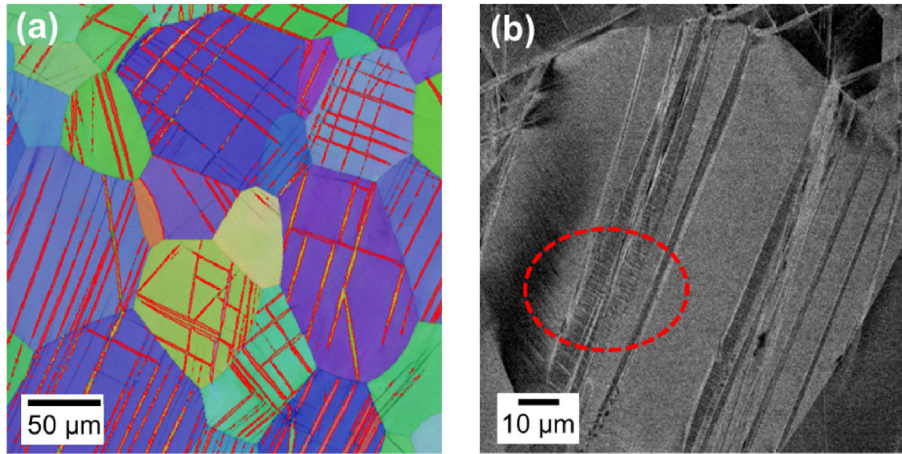


**Fig. 3.** EBSD mapping of Ti513 deformed at a strain of 10% (a) IPF + IQ. (b) BSE image.  $\{332\}$  twin boundaries are marked by red solid lines in (a) and the band-like structures are marked by dashed red circle in (b). (For interpretation of the references to colour in this figure legend, the reader is referred to the Web version of this article.)

secondary deformation products inside of the coarse twins which also contributes to the enhanced strain hardening rate and plasticity. As these fine secondary products are beyond the resolution of EBSD, TEM was employed to further analyse these fine structures.

Fig. 4a–k give TEM micrographs of internal deformation bands in the 10% strained sample. Within the primary  $\{332\}\langle 113\rangle$  twin, the bright-field TEM image (Fig. 4a) clearly reveals the existence of secondary deformation bands inside. The SAED pattern in Fig. 4b indicates that there are four sets of diffraction patterns along  $\langle 110\rangle$  zone axis and they are highlighted in red, blue, green and yellow solid rectangles respectively. The corresponding dark-field images taken from the solid circles confirm the formation of three different

deformation products (Fig. 4c–f). According to the key diagrams in Fig. 4g–i, these deformation products are defined as  $\{112\}\langle 111\rangle$  twin and two different variants of  $\{332\}\langle 113\rangle$  twins respecting to the primary deformation band (Fig. 4c). Interestingly, the schematic diagrams shown in Fig. 4j and 4k reveal that one of secondary  $\{332\}\langle 113\rangle$  twins shown in Fig. 4f also fulfils the relationship of  $\{112\}\langle 111\rangle$  and  $\{332\}\langle 113\rangle$  twinning system with two other twins. Considering the geometric relationship between these band structures, the sequence of activation can be concluded as follows: primary  $\{332\}\langle 113\rangle$  twins are activated first during the early stage of the plastic deformation. An increase of strain results in the growth of primary  $\{332\}\langle 113\rangle$  twins and the activation secondary

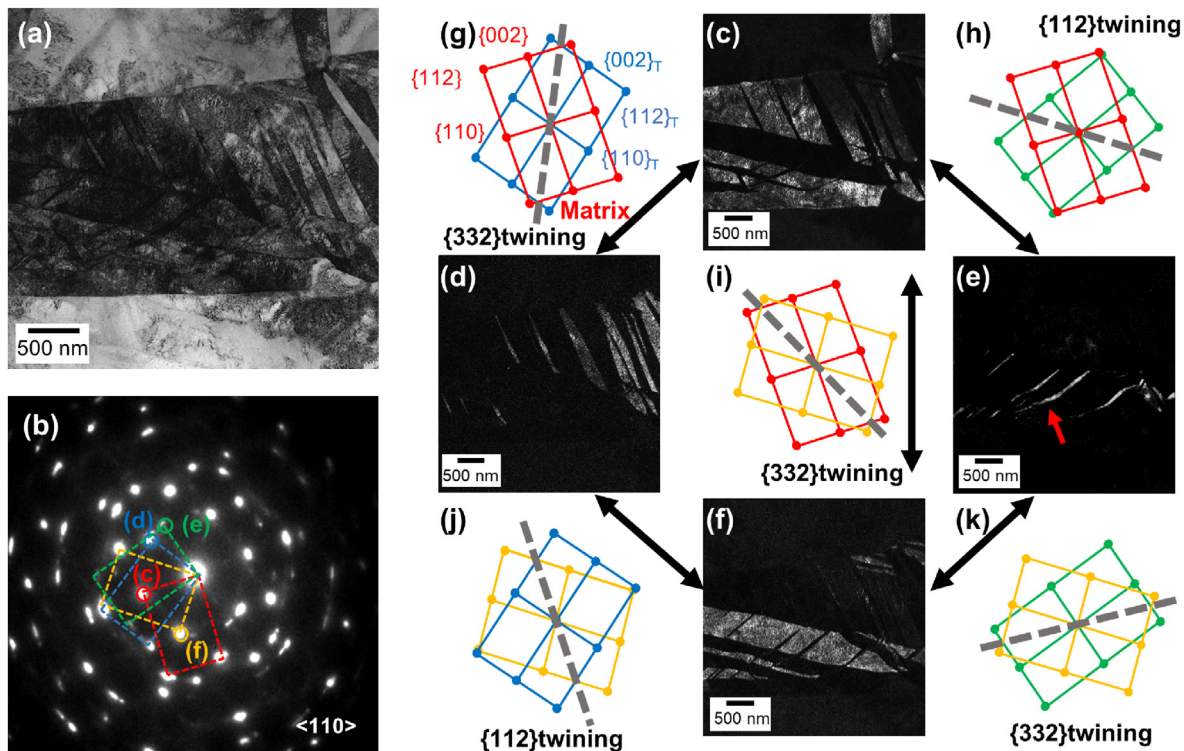


**Fig. 4.** (a) Bright field image of a primary deformation twin. (b) Corresponding SAED pattern inside the band along  $[110]$  zone axis. (c–f) Dark field images taken from the solid circles indicated in (b). (g–k) The schematic illustration of relationships between deformation bands.

{332}<113> twins in coarse primary {332}<113> twins. With a further increase of strain, ternary {112}<111> twins are nucleated in secondary {332} type twins. Our primary twins have relatively large sizes (width between 1 and 3  $\mu\text{m}$ ), which is like a subgrain in the recrystallized grains. The formation of secondary and tertiary twins efficiently subdivide the micro twins down to the nanoscale (Fig. 4c). Thus, the continuous activation of subsequent deformation products could strengthen the primary twins and together contribute to a long-standing dynamic Hall-Petch effect, which is responsible for the high and stable work hardening rates observed between 5% and 12% strain (Fig. 2a). The formation of primary {332}<113> twins in metastable Ti alloys is quite complicated and still not fully understood. As previously reported, the nucleation and propagation of twins are a function of grain orientation as well as other deformation products, such as SIM and {112}<111> twins [12,20,35]. The sub-twins appear to be a result of enhanced local stress conditions and strain accommodation. Besides, the {112}<111> twin is known to have higher CRSS than that of {332}<113> twin [36]. Thus, the formation of ternary {112}<111> twin is attributed to the synergistic effect of enhanced local stress and higher Schmid factor (SF) due to local plastic deformation resulted grain reorientations. This explains why {112}<111> always nucleate inside secondary twins [37]. Therefore, the in-situ evolution of SF inside the primary deformation bands should be investigated using precession diffraction in the TEM.

The  $d$ -electron theory is the most popular current approach to design Ti alloy composition. The  $\overline{B}o - \overline{M}d$  diagram derived from the cluster DV-X $\alpha$  method clearly demonstrates the transition of deformation mechanism in metastable  $\beta$  Ti alloys, i.e., SIM, twinning and dislocation slip [3,6]. Notably, the calculated  $\overline{B}o$  and  $\overline{M}d$  of Ti513 are 2.787 and 2.398 respectively. Their position in the diagram is located in martensite, suggesting the deformation mechanisms should be dominated by SIM. In contrast, EBSD and TEM results show that both {332}<113> and {112}<111> twins are activated during deformation, and there is no evidence of the formation of SIM. More recent research also found that the part of  $\overline{B}o - \overline{M}d$  diagram with low values, especially the martensite zone, still needs more compositions investigations to perfect the boundary position [38]. It was reported that Sn could decrease the martensite start temperature ( $M_s$ ) and acts as a  $\beta$  stabilizer in some cases [3,13]. Thus one reason is believed that the addition of Sn in Ti513 inhibits the initiation of SIM. Another possibility can be associated with the reversion of martensite that transfers to {332}<113> twin when the stress is released, which has been demonstrated via in situ synchrotron x-ray diffraction [39].

Previous works have suggested that Sn and Zr can effectively facilitate the suppression of  $\omega$  phase via suppressing the collapse of {222} $_{\beta}$  planes [14,15,40,41]. In the current Ti513 alloy, the addition of Sn is responsible for the absence of athermal  $\omega$  phase. It not only decreases the Young's modulus to 52 GPa, but also minimizes the risk of embrittlement due to room aging of beta Ti alloys, which is significantly essential for long-term implantation [2,42]. Furthermore, the ultra-low Young's modulus can also be attributed to the electron/atom ratio ( $e/a$ , average valence electron per atom) of  $\sim 4.14$ . Decreasing  $e/a$  is favorable to get a low Young's modulus due to the correlated lattice softening effect of metastable  $\beta$  Ti alloys, but negatively affected by the formation of  $\alpha''$ / $\alpha'$  and  $\omega$  related to the increased  $\beta$  phase instability [5]. Thus, with a low  $e/a$  value, a minimum Young's modulus would be achieved when these metastable phases are completely suppressed [43]. The high yield strength is believed to be associated with the solid solution hardening effects of Fe. In a Ti–10Mo alloy, the addition of 2 wt% of Fe increased the yield strength from 572 to 902 MPa by improving the CRSS for twinning [44]. It is well known that the deformation mechanisms of metastable  $\beta$  Ti alloys change from SIM and

twinning to slip as the  $\beta$  phase stability is increased. However, Fe is a eutectoid  $\beta$  phase stabilizer. During solidification, or heat treatment at high temperature, the addition of too much Fe leads to the risk of forming "beta fleck", which is caused by segregation of  $\beta$  stabilizers and can facilitate the crack nucleation during deformation, deteriorating mechanical properties [45,46]. In the current work, the amount of Fe was chosen to be 1% to avoid segregation and consequent poor plasticity. However, it was the synergy of the combined addition of Sn and Fe which gave the excellent low Young's modulus, high yield strength, and enhanced plasticity. This strategy also has the potential to be introduced to other binary metastable Ti alloys, e.g., Ti–Nb and Ti–Ta.

#### 4. Conclusions

In summary, a new metastable  $\beta$  Ti alloy, Ti–5Mo–Fe–3Sn (Ti513) has been successfully developed. It exhibits a very low Young's modulus of 52 GPa, an attractive uniform elongation of 15% as well as high yield strength of 740 MPa, resulting in competitive elastic admissible strain (1.42%) comparing to recent established biomedical Ti alloys. The addition of Sn and Fe is found to suppress the formation of athermal  $\omega$  phase and improved yield strength. A high elastic admissible strain is thus promoted. The enhanced plasticity is attributed to the network of primary {332} twins as well as the activation of various sub-twins, i.e., {332}<113> and {112}<111> twins. This is the first time to report the primary {332} twin consisted of two secondary {332} twins and {112} twins, which provides a new strain mediation strategy in metastable  $\beta$  Ti alloys.

#### CRediT authorship contribution statement

**Yidong Xu:** Conceptualization, Methodology, Software, Writing - original draft. **Junheng Gao:** Investigation, Supervision. **Yuhe Huang:** Investigation. **W. Mark Rainforth:** Supervision, Writing - review & editing.

#### Acknowledgements

This work is supported by the UK EPSRC project "Designing Alloys for Resource Efficiency (DARE)", EP/L025213/1. The authors would like to thank Mr Neil Hind for heat treatment and hot rolling. Helpful discussions and assistance of Dr J.W Xi are also acknowledged.

#### Appendix A. Supplementary data

Supplementary data to this article can be found online at <https://doi.org/10.1016/j.jallcom.2020.155391>.

#### References

- [1] M. Geetha, A.K. Singh, R. Asokamani, A.K. Gogia, Ti based biomaterials, the ultimate choice for orthopaedic implants - a review, *Prog. Mater. Sci.* 54 (2009) 397–425, <https://doi.org/10.1016/j.pmatsci.2008.06.004>.
- [2] M. Abdel-Hady Gepreel, M. Niinomi, Biocompatibility of Ti-alloys for long-term implantation, *J. Mech. Behav. Biomed. Mater.* 20 (2013) 407–415, <https://doi.org/10.1016/j.jmbbm.2012.11.014>.
- [3] M. Abdel-Hady, K. Hinoshita, M. Morinaga, General approach to phase stability and elastic properties of  $\beta$ -type Ti-alloys using electronic parameters, *Scripta Mater.* 55 (2006) 477–480, <https://doi.org/10.1016/j.scriptamat.2006.04.022>.
- [4] S.J. Li, T.C. Cui, Y.L. Hao, R. Yang, Fatigue properties of a metastable  $\beta$ -type titanium alloy with reversible phase transformation, *Acta Biomater.* 4 (2008) 305–317, <https://doi.org/10.1016/j.actbio.2007.09.009>.
- [5] Y.L. Hao, S.J. Li, S.Y. Sun, C.Y. Zheng, R. Yang, Elastic deformation behaviour of Ti–24Nb–4Zr–7.9Sn for biomedical applications, *Acta Biomater.* 3 (2007) 277–286, <https://doi.org/10.1016/j.actbio.2006.11.002>.
- [6] D. Kuroda, M. Niinomi, M. Morinaga, Y. Kato, T. Yashiro, Design and mechanical properties of new  $\beta$  type titanium alloys for implant materials, *Mater.*

- Sci. Eng. 243 (1998) 244–249, [https://doi.org/10.1016/s0921-5093\(97\)00808-3](https://doi.org/10.1016/s0921-5093(97)00808-3).
- [7] K. Hagihara, T. Nakano, Experimental clarification of the cyclic deformation mechanisms of  $\beta$ -type Ti-Nb-Ta-Zr alloy single crystals developed for the single-crystalline implant, *Int. J. Plast.* 98 (2017) 27–44, <https://doi.org/10.1016/j.ijplas.2017.06.006>.
- [8] P. Li, X. Ma, T. Tong, Y. Wang, Microstructural and mechanical properties of  $\beta$ -type Ti–Mo–Nb biomedical alloys with low elastic modulus, *J. Alloys Compd.* 815 (2020) 152412, <https://doi.org/10.1016/j.jallcom.2019.152412>.
- [9] S. Guo, Y. Shi, G. Liu, R. Wu, R. Luo, C.T. Peng, Q. Meng, X. Cheng, X. Zhao, Design and fabrication of a ( $\beta$ - $\alpha'$ ) dual-phase Ti-Nb-Sn alloy with linear deformation behavior for biomedical applications, *J. Alloys Compd.* 805 (2019) 517–521, <https://doi.org/10.1016/j.jallcom.2019.07.109>.
- [10] M. Marteleur, F. Sun, T. Gloriant, P. Vermaut, P.J. Jacques, F. Prima, On the design of new  $\beta$ -metastable titanium alloys with improved work hardening rate thanks to simultaneous TRIP and TWIP effects, *Scripta Mater.* 66 (2012) 749–752, <https://doi.org/10.1016/j.scriptamat.2012.01.049>.
- [11] F. Sun, J.Y. Zhang, M. Marteleur, T. Gloriant, P. Vermaut, D. Laillé, P. Castany, C. Curfs, P.J. Jacques, F. Prima, Investigation of early stage deformation mechanisms in a metastable  $\beta$  titanium alloy showing combined twinning-induced plasticity and transformation-induced plasticity effects, *Acta Mater.* 61 (2013) 6406–6417, <https://doi.org/10.1016/j.actamat.2013.07.019>.
- [12] J. Gao, Y. Huang, D. Guan, A.J. Knowles, L. Ma, D. Dye, W.M. Rainforth, Deformation mechanisms in a metastable beta titanium twinning induced plasticity alloy with high yield strength and high strain hardening rate, *Acta Mater.* 152 (2018) 301–314, <https://doi.org/10.1016/j.actamat.2018.04.035>.
- [13] S. Cai, L. Wang, J.E. Schaffer, J. Gao, Y. Ren, Influence of Sn on martensitic beta Ti alloys, *Mater. Sci. Eng.* 743 (2019) 764–772, <https://doi.org/10.1016/j.msea.2018.11.095>.
- [14] M.F. Ijaz, H.Y. Kim, H. Hosoda, S. Miyazaki, Effect of Sn addition on stress hysteresis and superelastic properties of a Ti-15Nb-3Mo alloy, *Scripta Mater.* (2014) 72–73, <https://doi.org/10.1016/j.scriptamat.2013.10.007>, 29–32.
- [15] E.L. Pang, E.J. Pickering, S.I. Baik, D.N. Seidman, N.G. Jones, The effect of zirconium on the omega phase in Ti-24Nb-[0–8]Zr (at.%) alloys, *Acta Mater.* 153 (2018) 62–70, <https://doi.org/10.1016/j.actamat.2018.04.016>.
- [16] S.K. Sikka, Y.K. Vohra, R. Chidambaram, Omega phase in materials, *Prog. Mater. Sci.* 27 (1982) 245–310, [https://doi.org/10.1016/0079-6425\(82\)90002-0](https://doi.org/10.1016/0079-6425(82)90002-0).
- [17] A.A. Salem, S.R. Kalidindi, R.D. Doherty, Strain hardening of titanium: role of deformation twinning, *Acta Mater.* 51 (2003) 4225–4237, [https://doi.org/10.1016/S1359-6454\(03\)00239-8](https://doi.org/10.1016/S1359-6454(03)00239-8).
- [18] J.W. Christian, S. Mahajan, Deformation twinning, *Prog. Mater. Sci.* 39 (1995) 1–157, [https://doi.org/10.1016/0079-6425\(94\)00007-7](https://doi.org/10.1016/0079-6425(94)00007-7).
- [19] X. Min, X. Chen, S. Emura, K. Tsuchiya, Mechanism of twinning-induced plasticity in  $\beta$ -type Ti-15Mo alloy, *Scripta Mater.* 69 (2013) 393–396, <https://doi.org/10.1016/j.scriptamat.2013.05.027>.
- [20] L. Liliensten, Y. Danard, C. Brozek, S. Mantri, P. Castany, T. Gloriant, P. Vermaut, F. Sun, R. Banerjee, F. Prima, On the heterogeneous nature of deformation in a strain-transformable beta metastable Ti-V-Cr-Al alloy, *Acta Mater.* 162 (2019) 268–276, <https://doi.org/10.1016/j.actamat.2018.10.003>.
- [21] S. Ozan, J. Lin, Y. Li, R. Ipek, C. Wen, Development of Ti-Nb-Zr alloys with high elastic admissible strain for temporary orthopedic devices, *Acta Biomater.* 20 (2015) 176–187, <https://doi.org/10.1016/j.actbio.2015.03.023>.
- [22] A. Nocivini, I. Cinca, D. Raducanu, V.D. Cojocaru, I.A. Popovici, Mechanical properties of a Gum-type Ti–Nb–Zr–Fe–O alloy, *Int. J. Miner. Metall. Mater.* 24 (2017) 909–917, <https://doi.org/10.1007/s12613-017-1477-3>.
- [23] M. Niinomi, Mechanical properties of biomedical titanium alloys, *Mater. Sci. Eng.* 243 (1998) 231–236, [https://doi.org/10.1016/S0921-5093\(97\)00806-X](https://doi.org/10.1016/S0921-5093(97)00806-X).
- [24] M.R. Dal Bo, C.A.F. Salvado, M.G. Mello, D.D. Lima, G.A. Faria, A.J. Ramirez, R. Caram, The effect of Zr and Sn additions on the microstructure of Ti-Nb-Fe gum metals with high elastic admissible strain, *Mater. Des.* 160 (2018), <https://doi.org/10.1016/j.matdes.2018.10.040>.
- [25] A. Biesiekierski, J. Lin, Y. Li, D. Ping, Y. Yamabe-Mitarai, C. Wen, Investigations into Ti-(Nb,Ta)-Fe alloys for biomedical applications, *Acta Biomater.* 32 (2016) 336–347, <https://doi.org/10.1016/j.actbio.2015.12.010>.
- [26] T. Saito, T. Furuta, J.-H. Hwang, S. Kuramoto, K. Nishino, N. Suzuki, R. Chen, A. Yamada, K. Ito, Y. Seno, T. Nonaka, H. Ikehata, N. Nagasako, C. Iwamoto, Y. Ikuhara, T. Sakuma, Multifunctional alloys obtained via a dislocation-free plastic deformation mechanism, *Science* 300 (2003) 464–467, <https://doi.org/10.1126/science.1081957>.
- [27] X. Ji, S. Emura, T. Liu, K. Suzuta, X. Min, K. Tsuchiya, Effect of oxygen addition on microstructures and mechanical properties of Ti-7.5Mo alloy, *J. Alloys Compd.* 737 (2018) 221–229, <https://doi.org/10.1016/j.jallcom.2017.12.072>.
- [28] X. Min, P. Bai, S. Emura, X. Ji, C. Cheng, B. Jiang, K. Tsuchiya, Effect of oxygen content on deformation mode and corrosion behavior in  $\beta$ -type Ti-Mo alloy, *Mater. Sci. Eng.* 684 (2017) 534–541, <https://doi.org/10.1016/j.msea.2016.12.062>.
- [29] Y. Abdelrhman, M.A.H. Gepreel, S. Kobayashi, S. Okano, T. Okamoto, Biocompatibility of new low-cost ( $\alpha$  +  $\beta$ )-type Ti-Mo-Fe alloys for long-term implantation, *Mater. Sci. Eng. C* 99 (2019) 552–562, <https://doi.org/10.1016/j.jmsec.2019.01.133>.
- [30] Y.L. Zhou, M. Niinomi, Ti-25Ta alloy with the best mechanical compatibility in Ti-Ta alloys for biomedical applications, *Mater. Sci. Eng. C* 29 (2009) 1061–1065, <https://doi.org/10.1016/j.jmsec.2008.09.012>.
- [31] Y.L. Zhou, M. Niinomi, Microstructures and mechanical properties of Ti-50 mass% Ta alloy for biomedical applications, *J. Alloys Compd.* 466 (2008) 535–542, <https://doi.org/10.1016/j.jallcom.2007.11.090>.
- [32] E. Bertrand, T. Gloriant, D.M. Gordin, E. Vasilescu, P. Drob, C. Vasilescu, S.I. Drob, Synthesis and characterisation of a new superelastic Ti-25Ta-25Nb biomedical alloy, *J. Mech. Behav. Biomed. Mater.* 3 (2010) 559–564, <https://doi.org/10.1016/j.jmbbm.2010.06.007>.
- [33] P.F. Santos, M. Niinomi, K. Cho, M. Nakai, H. Liu, N. Ohtsu, M. Hirano, M. Ikeda, T. Narushima, Microstructures, mechanical properties and cytotoxicity of low cost beta Ti-Mn alloys for biomedical applications, *Acta Biomater.* 26 (2015) 366–376, <https://doi.org/10.1016/j.actbio.2015.08.015>.
- [34] P. Fernandes Santos, M. Niinomi, H. Liu, K. Cho, M. Nakai, A. Trenggono, S. Champagne, H. Hermawan, T. Narushima, Improvement of microstructure, mechanical and corrosion properties of biomedical Ti-Mn alloys by Mo addition, *Mater. Des.* 110 (2016) 414–424, <https://doi.org/10.1016/j.matdes.2016.07.115>.
- [35] M.J. Lai, C.C. Tasan, D. Raabe, On the mechanism of {332} twinning in metastable  $\beta$  titanium alloys, *Acta Mater.* 111 (2016) 173–186, <https://doi.org/10.1016/j.actamat.2016.03.040>.
- [36] L. Ren, W. Xiao, C. Ma, R. Zheng, L. Zhou, Development of a high strength and high ductility near  $\beta$ -Ti alloy with twinning induced plasticity effect, *Scripta Mater.* 156 (2018) 47–50, <https://doi.org/10.1016/j.scriptamat.2018.07.012>.
- [37] S.A. Mantri, F. Sun, D. Choudhuri, T. Alam, B. Gwalani, F. Prima, R. Banerjee, Deformation induced hierarchical twinning coupled with omega transformation in a metastable  $\beta$ -Ti alloy, *Sci. Rep.* 9 (2019) 1334, <https://doi.org/10.1038/s41598-018-37865-0>.
- [38] C.H. Wang, A.M. Russell, G.H. Cao, A semi-empirical approach to the prediction of deformation behaviors of  $\beta$ -Ti alloys, *Scripta Mater.* 158 (2019) 62–65, <https://doi.org/10.1016/j.scriptamat.2018.08.035>.
- [39] P. Castany, Y. Yang, E. Bertrand, T. Gloriant, Reversion of a parent {130}<310> $\alpha'$  martensitic twinning system at the origin of {332}<113> $\beta$  twins observed in metastable  $\beta$  titanium alloys, *Phys. Rev. Lett.* 117 (2016) 245501, <https://doi.org/10.1103/PhysRevLett.117.245501>.
- [40] Y. Zheng, R.E.A. Williams, S. Nag, R. Banerjee, H.L. Fraser, D. Banerjee, The effect of alloy composition on instabilities in the  $\beta$  phase of titanium alloys, *Scripta Mater.* 116 (2016) 49–52, <https://doi.org/10.1016/j.scriptamat.2016.01.024>.
- [41] P. Wang, M. Todai, T. Nakano,  $\omega$ -phase transformation and lattice modulation in biomedical  $\beta$ -phase Ti-Nb-Al alloys, *J. Alloys Compd.* 766 (2018) 511–516, <https://doi.org/10.1016/j.jallcom.2018.06.266>.
- [42] Y. Al-Zain, Y. Sato, H.Y. Kim, H. Hosoda, T.H. Nam, S. Miyazaki, Room temperature aging behavior of Ti-Nb-Mo-based superelastic alloys, *Acta Mater.* 60 (2012) 2437–2447, <https://doi.org/10.1016/j.actamat.2011.12.033>.
- [43] P. Wang, M. Todai, T. Nakano, Beta titanium single crystal with bone-like elastic modulus and large crystallographic elastic anisotropy, *J. Alloys Compd.* 782 (2019) 667–671, <https://doi.org/10.1016/j.jallcom.2018.12.236>.
- [44] I. Gutierrez-Urrutia, C.L. Li, S. Emura, X. Min, K. Tsuchiya, Study of {332}<113> twinning in a multilayered Ti-10Mo-xFe (x = 1–3) alloy by ECCI and EBSD, *Sci. Technol. Adv. Mater.* 17 (2016) 220–228, <https://doi.org/10.1080/14686996.2016.1177439>.
- [45] W.D. Zeng, Y.G. Zhou, Effect of beta flecks on mechanical properties of Ti–10V–2Fe–3Al alloy, *Mater. Sci. Eng.* 260 (1999) 203–211, [https://doi.org/10.1016/s0921-5093\(98\)00954-x](https://doi.org/10.1016/s0921-5093(98)00954-x).
- [46] C.E. Shamblen, Minimizing beta flecks in the ti-17 alloy, *Metall. Mater. Trans. B* 28 (1997) 899–903, <https://doi.org/10.1007/s11663-997-0017-3>.